An extended actuator cylinder model

Actuator-in-actuator cylinder (AC-squared) model

De Tavernier, Delphine; Ferreira, Carlos

DOI
10.1002/we.2340

Publication date
2019

Document Version
Final published version

Published in
Wind Energy

Citation (APA)
De Tavernier, D., & Ferreira, C. (2019). An extended actuator cylinder model: Actuator-in-actuator cylinder (AC-squared) model. *Wind Energy*, *22*(8), 1058-1070. https://doi.org/10.1002/we.2340

Received: 18 August 2018 | Revised: 7 February 2019 | Accepted: 4 March 2019
DOI: 10.1002/we.2340

WILEY

RESEARCH ARTICLE

An extended actuator cylinder model: Actuator-in-actuator cylinder (AC-squared) model

Delphine De Tavernier | **Carlos Ferreira**

Wind Energy Research Institute, Faculty of Aerospace Engineering, Delft University of Technology, Delft 2496HS, The Netherlands

Correspondence
Delphine De Tavernier, Wind Energy Section, Faculty of Aerospace Engineering, Delft University of Technology, Kluyverweg 1, Delft 2629HS, The Netherlands.
Email: d.a.m.detavernier@tudelft.nl

Abstract

In this paper, the actuator-in-actuator cylinder (AC-squared) model is presented. This model is an extension of the original actuator cylinder model of Madsen and is capable of modelling the effect of a two concentric actuation surfaces in 2D. The induced velocity at every point in the 2D field is affected by the force field acting on the two actuator cylinders. The equations are derived, and a model verification is performed using analytical solutions of flows, proof of flow equivalence, and using OpenFOAM calculations. Finally, the model is applied to different case studies, and the results are compared with a time-dependent free wake vortex method.

KEYWORDS

actuator cylinder, double actuator, VAWT, vertical axis wind turbine

1 | INTRODUCTION

Compared with conventional horizontal axis wind turbines (HAWTs), vertical axis wind turbines (VAWTs) exhibit several advantages that make them attractive candidates for more efficient off-shore wind farms. In particular, the insensitivity to wind direction and the low center of gravity have caused a renewed surge of interest in VAWTs for floating, deep-offshore applications.[1]

To accelerate the adoption of the VAWT concept in the offshore wind industry, there is a need for a deeper understanding of their complex rotor aerodynamics. In most previous studies,[2,3] VAWTs have been idealized by modelling a single actuation surface, which coincides with the swept area of the rotor blades. Despite its relatively high accuracy and computational efficiency, this simplified approach is incapable of incorporating the effect of additional wind turbine components on the overall rotor aerodynamics, which could, however, play a significant role. For example, the effect of the struts or tower cannot be accounted for, nor could more unconventional VAWTs such as double-bladed concepts or the so-called butterfly turbine be modelled with these approaches. These applications are visualised in Figure 1. With this in mind, this research studies two concentric actuators: the actuator-in-actuator cylinder concept (AC-squared).

1.1 | Background

To model actuator-in-actuator applications, various simulation codes have been considered in literature, balancing accuracy with computational speed. The highest fidelity models, being 2D and 3D CFD models, allow the effect of the tower and struts on the VAWT loading and performance to be identified by simply introducing the geometry into the simulations. This is studied by various authors such as Rezaeiha et al[4] and Siddique et al.[5] Also actuator line and vortex models have been explored by, eg, Mendoza[6] to identify the effect of (inclined) struts.

Nomenclature: a, Induction factor [−]; c, Chord length [m]; C_P, Power coefficient [−]; C_T, Thrust coefficient [−]; C_Q, Torque coefficient [−]; D, Rotor diameter, $2R$ [m]; Q_n, Normal loading [−]; Q_t, Tangential loading [−]; R, Rotor radius [m]; V_x, X-velocity [m/s]; V_y, Y-velocity [m/s]; V, Relative velocity [m/s]; V_∞, Freestream velocity [m/s]; w, Induced velocity [−]; x, X-coordinate, X/R [−]; y, Y-coordinate, Y/R [−]; α, Angle of attack [°]; θ, Azimuthal angle [°]; σ, Rotor solidity, $Nc/2R$ [−]; λ, Tip speed ratio, $\omega R/V_{inf}$[−]; ω, Rotational speed [rad/s]; $\ldots_o$, Outer actuator [-]; $\ldots_i$, Inner actuator [-];

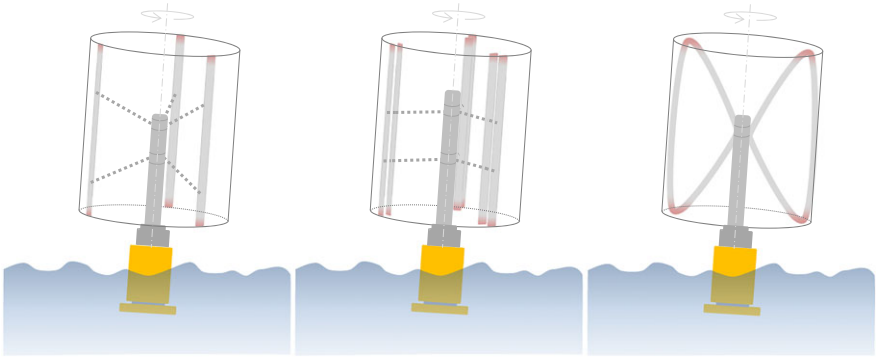

FIGURE 1 Applications of the actuator-in-actuator concept [Colour figure can be viewed at wileyonlinelibrary.com]

A lower fidelity but fast model is the streamtube model. A strut model has been implemented in this model by Moran,[7] who derived a correction coefficient for the drag. Inclined struts will also produce torque, and therefore, Goude[8] and later Hara et al[9] proposed a more general approach to include both lift and drag forces. They developed the double-multiple streamtube model with the purpose to extend the original multistreamtube model to simulate a 2D double-bladed VAWT. However, a major shortcoming of the streamtube model is that it does not account for the induction of the downwind part of the rotor on the upwind part of the rotor.

A model that does take into account the downstream induction on the upstream part but still offers a similar calculation speed as the streamtube model is the Actuator cylinder model developed by Madsen.[10] Although this model has not yet been extended to model the actuator-in-actuator concept, researchers such as Ning[11] and Li et al[12] already worked on the actuator cylinder theory for multiple VAWTs next to each other. In essence, the actuator-in-actuator concept could be seen as two side-by-side actuator cylinders with zero internal distance.

1.2 | Research objective

This research extends the original actuator cylinder model to simulate the actuator-in-actuator concept. It focusses on the development of the model and its verification, the presentation of an application of the actuator-in-actuator concept, and its comparison against other codes. The goal of this research can be formulated as follows:

1. Extending the original actuator cylinder (AC) model to the actuator-in-actuator cylinder (AC-squared) model.
2. Verifying the actuator-in-actuator cylinder model against analytical solutions and OpenFOAM (OF) calculations.
3. Demonstrating the actuator-in-actuator application using the actuator-in-actuator cylinder (AC-squared) model and comparing it against a free-wake vortex method.

2 | APPROACH AND METHODS

2.1 | Original actuator cylinder (AC) model

The actuator cylinder (AC) model, developed by Madsen,[13] is a 2D flow model extending the actuator disk concept.[14] An actuation surface is introduced that coincides with the swept area of the rotor, which is a cylindrical surface for a VAWT. The reaction of the blade forces (F_n and F_t) are applied on the flow as distributed body forces (Q_n and Q_t). The solution of the velocity field around the actuator cyinder builds on the 2D, steady, incompressible Euler equations, and the equation of continuity.[15] The induced velocities are prescribed by the volume forces and induced forces and consist of a linear and non-linear solution. The so-called *Mod-Lin* solution[16] uses only the linear version of the AC model and a correction to account for the non-linear part, instead of solving the computationally expensive non-linear solution. The non-linear part of the induced velocity is compensated using a correction factor k_a and is calculated based on the relation between the induction factor a and the thrust coefficient C_T. This relation includes that $C_T = 4a(1-a)$ for $a < 0.5$ as well as the Glauert correction for $a > 0.5$. This *Mod-Lin* solution method requires less resources and still delivers accurate results.[17] Figure 2A shows the 2D representation of an Actuator cylinder and presents the sign convention used in this work.

2.2 | Extended actuator-in-actuator cylinder (AC-squared) model

The actuator-in-actuator cylinder model builds further on the original AC model of Madsen.[13] The differences and applied adaptations will be highlighted in this section.

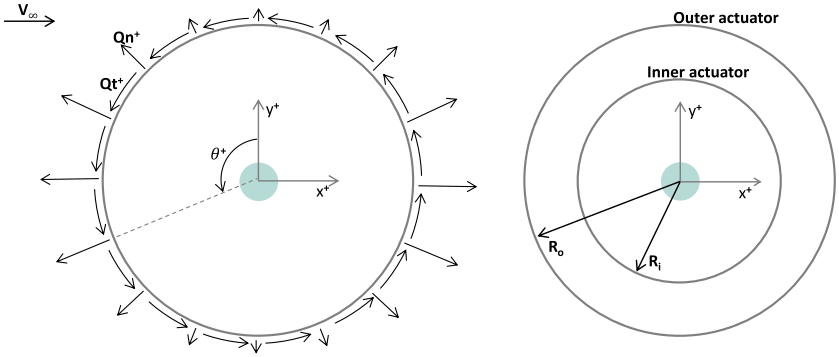

(A) *2D actuator cylinder* (B) *Actuator-in-actuator*

FIGURE 2 Actuator-in-actuator cylinder flow model and sign convention [Colour figure can be viewed at wileyonlinelibrary.com]

The induced velocity field in the AC-squared model is created by the force field of the inner as well as the outer actuator, as presented in Figure 2B. This means that the induced velocity field at any location in the 2D space is given by a component of the inner actuator and the outer actuator, as given by Figure 1 and Figure 2 in x- and y-direction, respectively. This is true because the *Mod-Lin* solution is linear. The induced velocities are normalised with the incoming velocity V_∞. The index *o* refers to the contribution of the outer actuator while index *i* refers to the contribution created by the inner actuator.

$$w_x(x,y) = w_{x,o}(x,y) + w_{x,i}(x,y) \tag{1}$$

$$w_y(x,y) = w_{y,o}(x,y) + w_{y,i}(x,y) \tag{2}$$

As in the original derivation, the actuator surface is discretised into N azimuthal panels. Each panel is prescribed with a piecewise constant loading Q_n and Q_t in the normal and tangential direction, respectively. In the original AC model, the induced velocity is only dependent on the normal loading. Madsen[13] and later Cheng et al[18] proposed to also include the tangential loading into the linear solution of the induced velocities; however, this only includes a minor contribution. The expressions for induced velocity at the cylinder surface depend on whether a point is evaluated inside or in the direct downstream of the Actuator cylinder. For evaluation points inside regions 1 to 5, additional terms apply. The different regions are specified in Figure 3. Applying the equation of the induced velocities derived by Madsen[13] on Equation 1 and Equation 2, Equation 3 and Equation 4 are obtained.

$$\begin{aligned}
w_x(x,y) = {} & \frac{1}{2\pi}\int_0^{2\pi} Q_{n_o}(\theta)\frac{(x_o+\sin(\theta))\sin(\theta)-(y_o-\cos(\theta))\cos(\theta)}{(x_o+\sin(\theta))^2+(y_o-\cos(\theta))^2}d\theta \\
& + \frac{1}{2\pi}\int_0^{2\pi} Q_{n_i}(\theta)\frac{(x_i+\sin(\theta))\sin(\theta)-(y_i-\cos(\theta))\cos(\theta)}{(x_i+\sin(\theta))^2+(y_i-\cos(\theta))^2}d\theta \\
& + \frac{1}{2\pi}\int_0^{2\pi} Q_{t_o}(\theta)\frac{(x_o+\sin(\theta))\cos(\theta)+(y_o-\cos(\theta))\sin(\theta)}{(x_o+\sin(\theta))^2+(y_o-\cos(\theta))^2}d\theta \\
& + \frac{1}{2\pi}\int_0^{2\pi} Q_{t_i}(\theta)\frac{(x_i+\sin(\theta))\cos(\theta)+(y_i-\cos(\theta))\sin(\theta)}{(x_i+\sin(\theta))^2+(y_i-\cos(\theta))^2}d\theta \\
& - Q_{n,o}(\cos^{-1}(y_o)) - Q_{t,o}(\cos^{-1}(y_o))\frac{y_o}{\sqrt{1-y_o^2}} \qquad \text{in region 1 to 5} \\
& + Q_{n,o}(-\cos^{-1}(y_o)) - Q_{t,o}(-\cos^{-1}(y_o))\frac{y_o}{\sqrt{1-y_o^2}} \qquad \text{in region 4 to 5} \\
& - Q_{n,i}(\cos^{-1}(y_i)) - Q_{t,i}(\cos^{-1}(y_i))\frac{y_i}{\sqrt{1-y_i^2}} \qquad \text{in region 2 to 4} \\
& + Q_{n,i}(-\cos^{-1}(y_i)) - Q_{t,i}(-\cos^{-1}(y_i))\frac{y_i}{\sqrt{1-y_i^2}} \qquad \text{in region 3 to 4}
\end{aligned} \tag{3}$$

$$\begin{aligned}
w_y(x,y) = {} & \frac{1}{2\pi}\int_0^{2\pi} Q_{n_o}(\theta)\frac{(x_o+\sin(\theta))\cos(\theta)+(y_o-\cos(\theta))\sin(\theta)}{(x_o+\sin(\theta))^2+(y_o-\cos(\theta))^2}d\theta \\
& + \frac{1}{2\pi}\int_0^{2\pi} Q_{n_i}(\theta)\frac{(x_i+\sin(\theta))\cos(\theta)+(y_i-\cos(\theta))\sin(\theta)}{(x_i+\sin(\theta))^2+(y_i-\cos(\theta))^2}d\theta \\
& - \frac{1}{2\pi}\int_0^{2\pi} Q_{t_o}(\theta)\frac{(x_o+\sin(\theta))\sin(\theta)-(y_o-\cos(\theta))\cos(\theta)}{(x_o+\sin(\theta))^2+(y_o-\cos(\theta))^2}d\theta \\
& - \frac{1}{2\pi}\int_0^{2\pi} Q_{t_i}(\theta)\frac{(x_i+\sin(\theta))\sin(\theta)-(y_i-\cos(\theta))\cos(\theta)}{(x_i+\sin(\theta))^2+(y_i-\cos(\theta))^2}d\theta
\end{aligned} \tag{4}$$

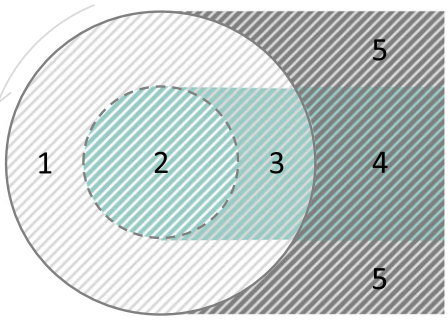

FIGURE 3 Representation of the different region in and around an actuator-in-actuator cylinder [Colour figure can be viewed at wileyonlinelibrary.com]

The variables x_o, y_o, x_i and y_i are non-dimensioned coordinates with respect to the radius of the outer and inner actuator, respectively. The volume forces $Q_{n,o}$, $Q_{t,o}$, $Q_{n,i}$, and $Q_{t,i}$ are given by Equation 5 to Equation 8, respectively. B is the number of blades, ρ the air density, and F_n and F_t are the normal and tangential forces acting on the actuator.

$$Q_{n,o}(\theta) = \frac{B \cdot F_{n,o}(\theta)}{2\pi R_o \rho V_\infty^2} \tag{5}$$

$$Q_{t,o}(\theta) = \frac{B \cdot F_{t,o}(\theta)}{2\pi R_o \rho V_\infty^2} \tag{6}$$

$$Q_{n,i}(\theta) = \frac{B \cdot F_{n,i}(\theta)}{2\pi R_i \rho V_\infty^2} \tag{7}$$

$$Q_{t,i}(\theta) = \frac{B \cdot F_{t,i}(\theta)}{2\pi R_i \rho V_\infty^2} \tag{8}$$

The correction factor k_a to account for the non-linear solution is given by a relation between the induction factor a and the thrust coefficient C_T. Note that C_T for both the outer and inner rotor is defined with respect to the outer rotor.

$$a = 0.089C_{T,o+i}^3 + 0.054C_{T,o+i}^2 + 0.251C_{T,o+i} - 0.002 \tag{9}$$

$$k_a = \frac{1}{1-a} \qquad \text{if} \quad a < 0.15 \tag{10}$$

$$k_a = \frac{1}{1-a} \cdot (0.65 + 0.35\exp(-4.5 \cdot (a - 0.15))) \qquad \text{if} \quad a > 0.15 \tag{11}$$

All simulations presented in this article are performed using 42 azimuthal sections. From the solution, the velocity field and streamlines are calculated for a domain with size $[-3D_o, 3D_o]$ in length and $[-2D_o, 2D_o]$ in height. The grid consists of 28 equally spaced cells in both directions.

2.3 | OpenFOAM (OF) model

To verify the actuator-in-actuator extension of the AC model, simulations are performed using computational fluid dynamics in OpenFOAM.[19] Simulations are made for a single AC as well as for the actuator-in-actuator concept for various thrust coefficients. A two-dimensional steady laminar solver, called *simpleFoam*, is used. The domain has size $[-15.5D_o, 20.5D_0]$ in width and $[-15.5D_o, 15.5D_0]$ in height. The grid is built using *blockMesh*, which decomposes the domain into a set of hexahedral blocks with straight and arc edges. In total, the domain consists of 276 000 cells with the main vortices and some cells for indication defined in Figure 4. The grid has shown to be dense enough and produce converged results on the x- and y-velocity behind the actuator with an accuracy below 1×10^{-3} for a thrust coefficient of 0.8. The actuator loading is applied in one thin row of cells as uniform body forces.

2.4 | U2DiVA model

For comparison purposes, the time-dependent model U2DiVA is used. U2DiVA is a two-dimensional panel/vortex model, developed by Ferreira.[20] It follows the Prandtl's lifting line theory and represents airfoils by a distribution of sources and doublets on the airfoil surface. The vortex is consequently shed into the wake with a velocity being a combination of the incoming wind speed and the induced velocity. The wake and velocity field around an arbitrary VAWT rotor is presented in Figure 5. From a convergence study on the power coefficient with the number of revolutions, it is concluded that 50 revolutions with a time step of 2.5° should suffice for medium to highly loaded cases. An extensive validation

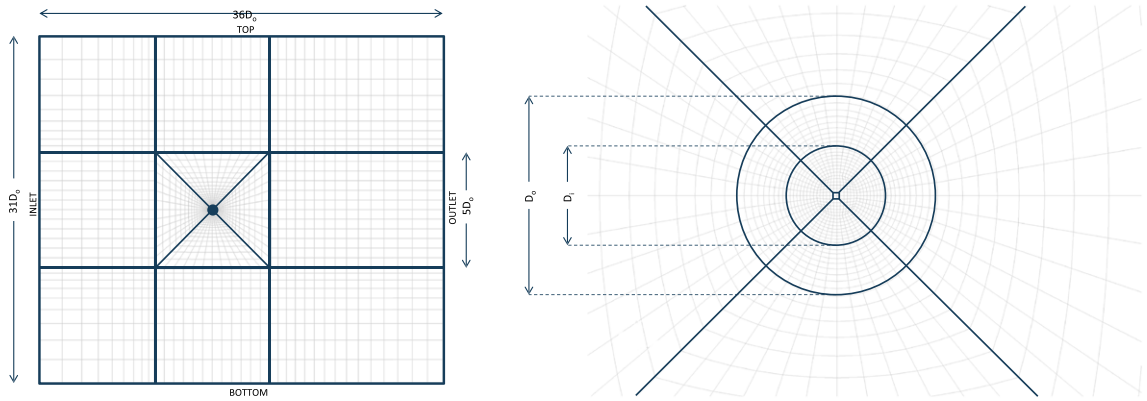

(A) *Complete domain* (B) *Zoom-in domain*

FIGURE 4 Representation of the domain size and grid used for the OpenFOAM calculations [Colour figure can be viewed at wileyonlinelibrary.com]

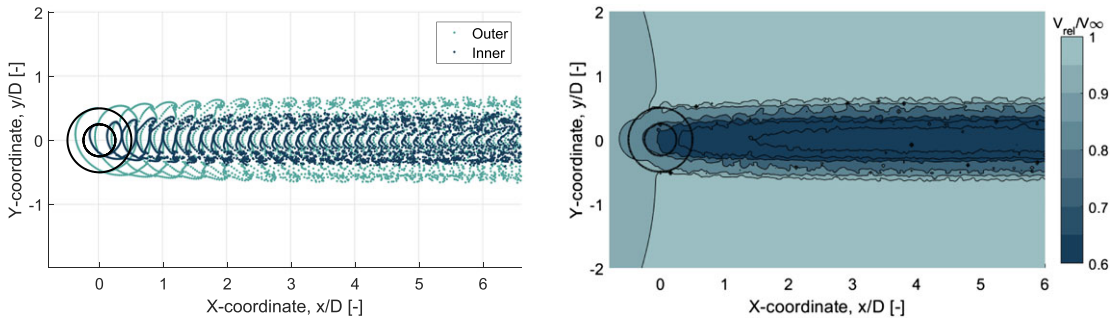

(A) *Wake* (B) *Velocity field*

FIGURE 5 Representation of the wake and velocity field of a two-bladed vertical axis wind turbine (VAWT) with NACA0015 airfoils. Tip speed ratio is 4, inner and outer solidity is 0.04, incoming velocity is 1m/s [Colour figure can be viewed at wileyonlinelibrary.com]

and comparison of this model with other aerodynamic models is provided in Ferreira.[21] The model can easily be adapted to calculate the velocity field around the actuator-in-actuator concept.

3 | RESULTS AND DISCUSSION

3.1 | Flowfield verification using analytical solutions

To verify the implementation of the AC model as well as the extended AC-squared model, flow cases with analytical solutions are studied. The force field of well-known examples are prescribed, and the flow field streamlines are computed.

The first case considers the flow around a cylinder, represented by a doublet being a combination of a source and sink of equal strength at infinitely small distance. At the wall of the cylinder, the radial velocity U_r is zero while the tangential velocity U_θ is proportional to U_∞ and $sin(\theta)$. The incoming velocity U_∞ is in the positive x-direction. This allows to say that the volume forces are proportional to U_θ^2 or in other words $U_\infty^2 sin^2(\theta)$. Using this force field as input for Q_n in the AC model allows to calculate the velocity around the cylinder and consequently the streamlines. The result is provided in Figure 6A where the left figure presents the force field introduced to the actuator surface and the right figure the steamlines. The results comply with the expectations. The same results are found for the force field applied to the inner rotor.

The second case can be considered as a simplified model of the flow around an airfoil. The airfoil is presented by a lifting surface and a force field is prescribed on the camber line of the airfoil with random strength. The results are provided in Figure 6(b) where the left figure presents the applied volume forces and the right figure the corresponding steamlines. The streamlines are deflected in a similar manner as around a potential airfoil. Again, the same results are found for the forcefield applied to the inner rotor.

The third case consists of applying a force field with a constant strength over the inner and outer actuator in normal direction. Because this force field does not create any vorticity, it is conservative, meaning the total work done in moving a particle between two points is independent of the taken path. As such the induced velocity will be zero according to the Biot-Savart law, and thus, no changes are expected to the incoming velocity field. In Figure 6C, the results calculated using the acuator-in-actuator cylinder model are provided. It presents the force field introduced to the model and the calculated steamlines.

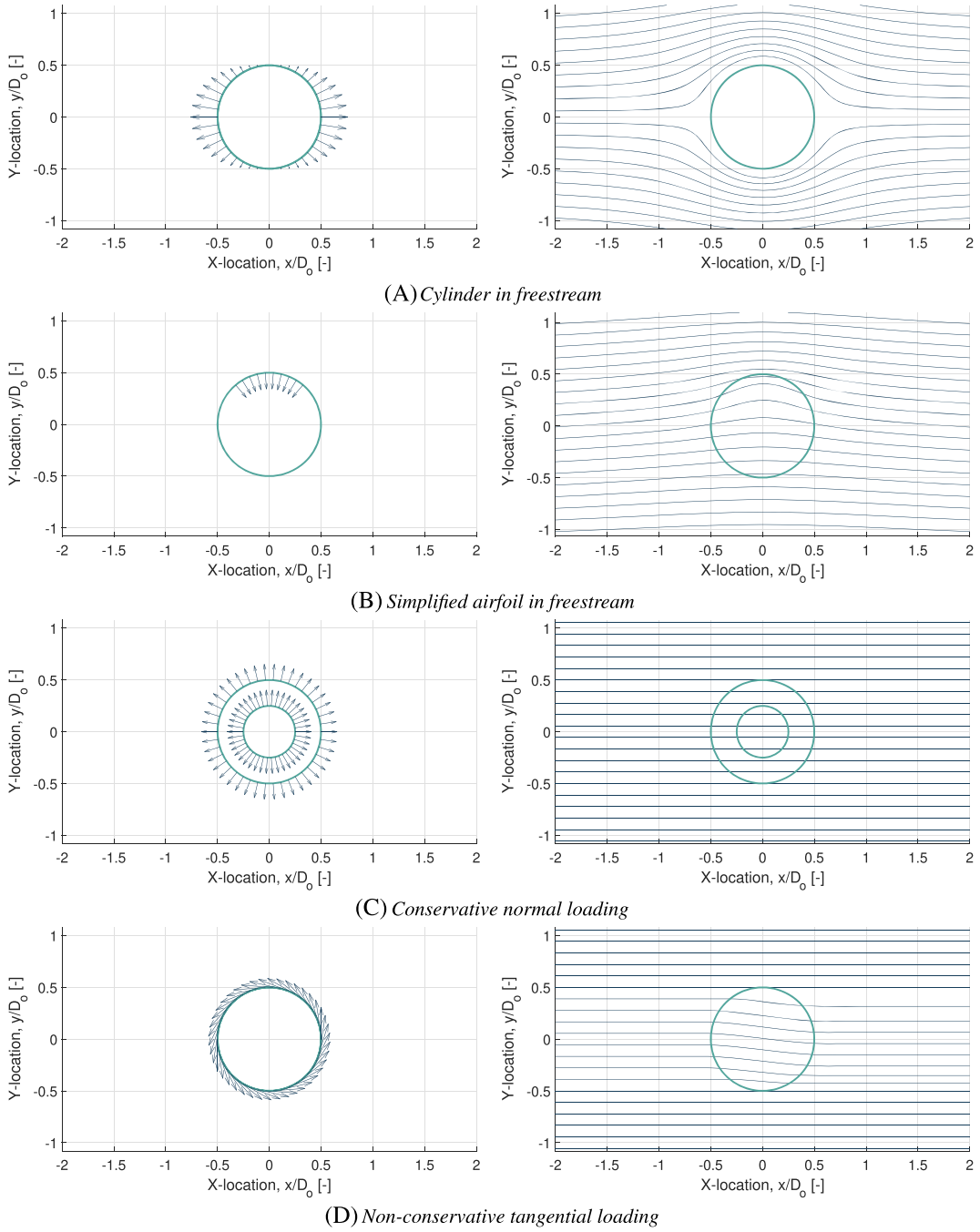

FIGURE 6 Flow around a well-known force field in uniform flow with analytical solutions to verify the actuator-in-actuator cylinder model [Colour figure can be viewed at wileyonlinelibrary.com]

Finally, a uniform force field with a random strength over the outer actuator in tangential direction is applied. This force field is nonconservative and should alter the velocity field. For volume forces working anticlockwise, the streamlines should be pushed down inside the actuator, and flattened again when leaving the actuator. In Figure 6D, the forcefield introduced to the model is presented as well as the streamlines.

With this final example, it is confirmed that the AC model is implemented correctly.

3.2 | Flow field verification using OpenFOAM calculations

To verify the extension of the AC model for the actuator-in-actuator concept further, a comparison is made between the flow field predicted by the model (AC-squared) and the field modelled with OpenFOAM (OF). To test the implementation step-by-step, a force field is applied first on the outer actuator only, then on the inner actuator and finally on both together. A uniform normal and tangential force field upwind and downwind is introduced with various strengths.

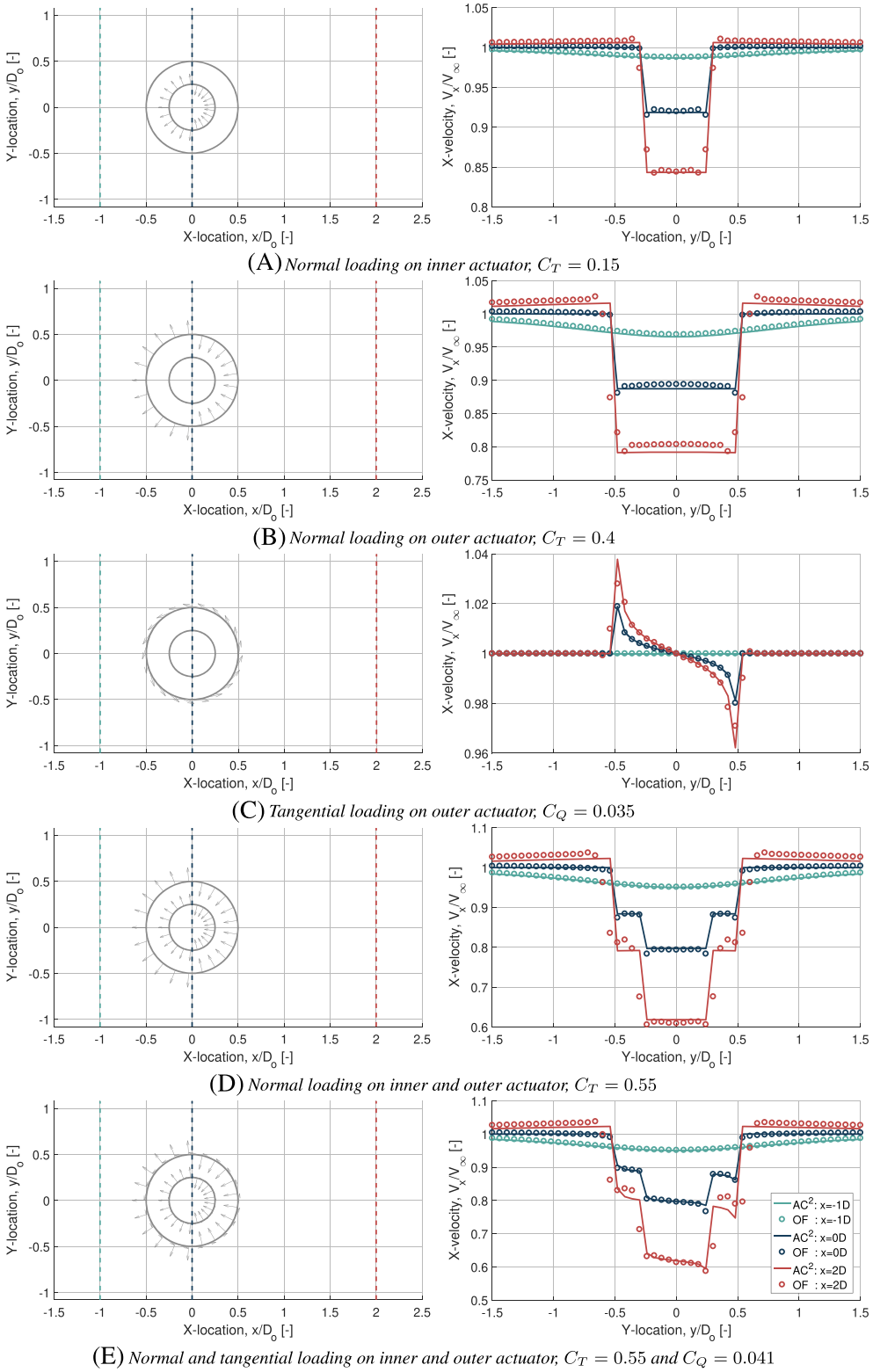

(A) *Normal loading on inner actuator,* $C_T = 0.15$

(B) *Normal loading on outer actuator,* $C_T = 0.4$

(C) *Tangential loading on outer actuator,* $C_Q = 0.035$

(D) *Normal loading on inner and outer actuator,* $C_T = 0.55$

(E) *Normal and tangential loading on inner and outer actuator,* $C_T = 0.55$ *and* $C_Q = 0.041$

FIGURE 7 X-velocity profile at three different x-locations for various loadings on inner and outer actuator calculated with the actuator-in-actuator cylinder (AC-squared) model and OpenFOAM (OF) [Colour figure can be viewed at wileyonlinelibrary.com]

One representative example comparing the AC-squared model and the OF results is provided in Figure 7 and Figure 8. In Figure 7, the x-velocity profile at three different x-locations for various loadings on the inner and outer actuator are provided. In Figure 8, the y-velocity profiles for the same loadings and at the same locations are presented. The three locations are: (1) one rotor diameter in front of the rotor, (2) at the rotor center, and (3) two rotor diameters behind the rotor. In the left figures, the loadings are visualised while at the right figures, the velocity profiles are displayed. The outer actuator is provided with a loading corresponding to a thrust coefficient of 0.4. The inner actuator has a thrust

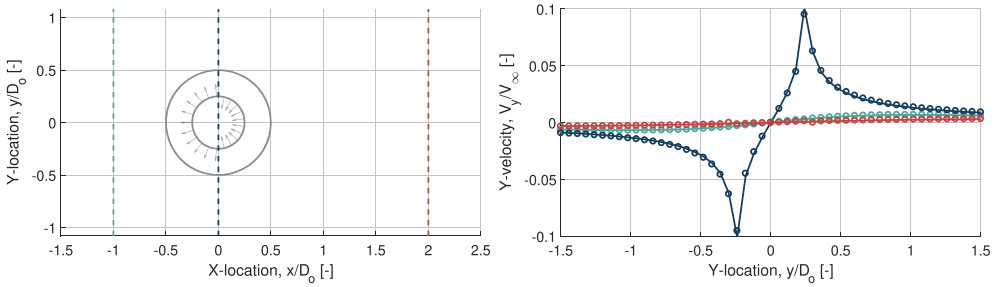

(A) *Normal loading on inner actuator,* $C_T = 0.15$

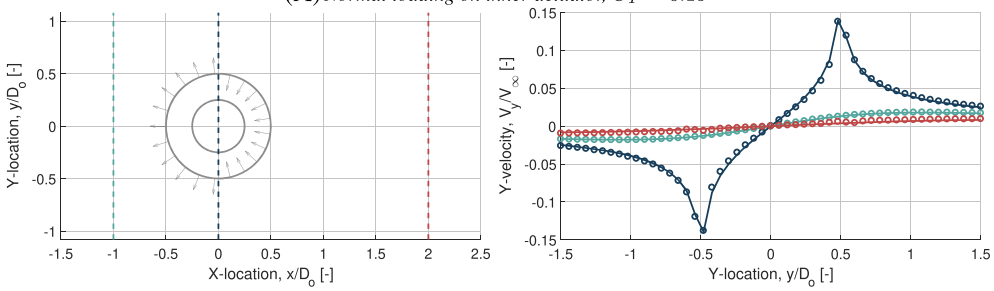

(B) *Normal loading on outer actuator,* $C_T = 0.4$

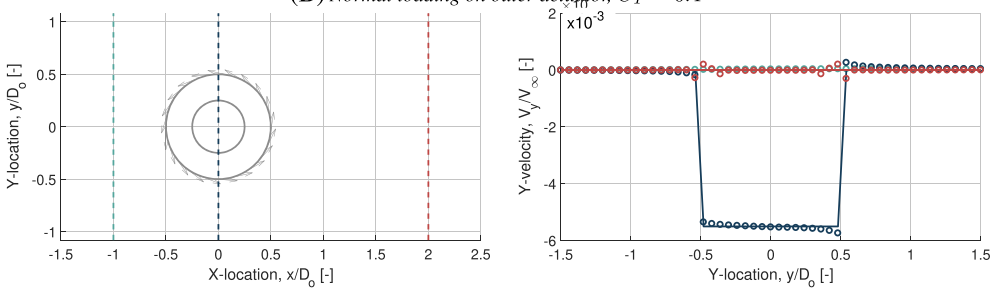

(C) *Tangential loading on outer actuator,* $C_Q = 0.035$

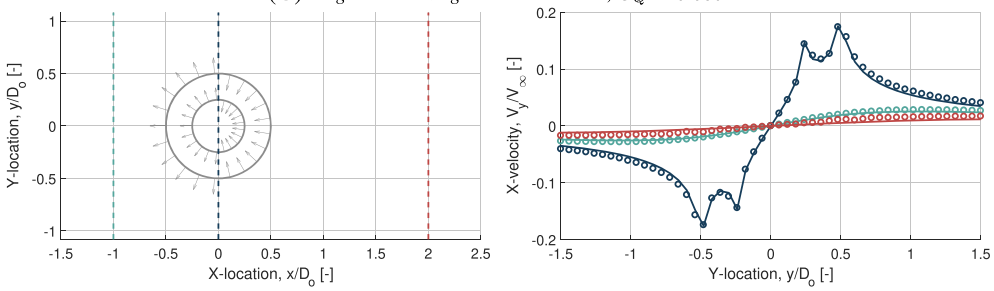

(D) *Normal loading on inner and outer actuator,* $C_T = 0.55$

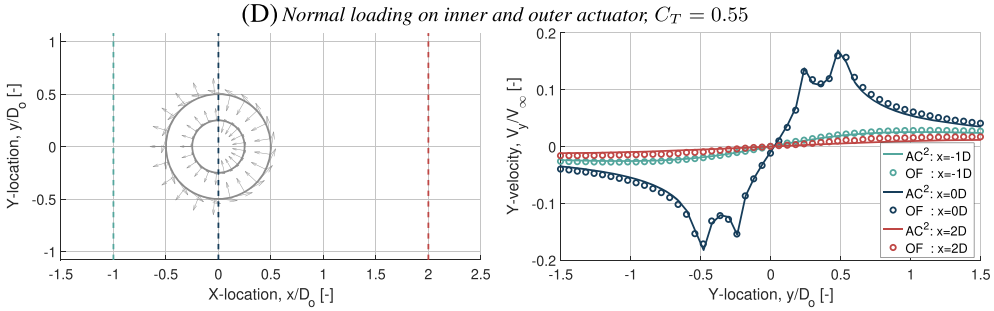

(E) *Normal and tangential loading on inner and outer actuator,* $C_T = 0.55$ *and* $C_Q = 0.041$

FIGURE 8 Y-velocity profile at three different x-locations for various loadings on inner and outer actuator calculated with the actuator-in-actuator cylinder (AC-squared) model and OpenFOAM (OF). [Colour figure can be viewed at wileyonlinelibrary.com]

coefficient of 0.15. The torque coefficient is one order smaller and equal to 0.035 for the outer actuator and 0.006 for the inner actuator. Note that the coefficients are all normalised with respect to the variables of the outer actuator.

From the results, some observations can be made. First of all, the overall behaviour of the x-velocity profiles and y-velocity profiles at the different x-locations, predicted by both models, compare well. The same trends are captured. From the x-velocity profiles, one can conclude that this velocity component is affected significantly by both the normal and tangential loadings. For all load forms, the profiles in front of the actuator and at the center of the actuator cylinder match almost identically. The induced velocity at the north and south of the actuator due to

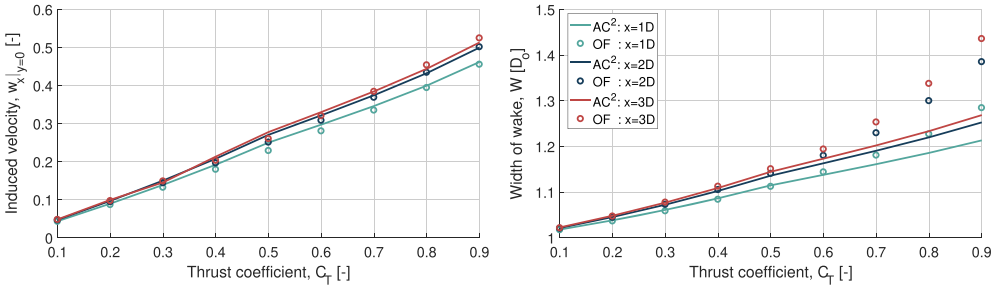

(A) *Induced velocity* (B) *Width of wake*

FIGURE 9 Induced velocity and width of the wake as a function of the thrust coefficient [Colour figure can be viewed at wileyonlinelibrary.com]

normal loadings are slightly underestimated by the AC-squared model causing the x-velocity to be slightly underpredicted. Behind the actuator cylinder, the induced x-velocity is overpredicted for the single actuator cylinder but slightly underpredicted for the actuator-in-actuator concept, however, still matching well. The effect of adding the tangential loading is captured well by the actuator-in-actuator model. The y-velocity profiles are mainly affected by the normal loadings and to a lower extend by the tangential loading. For the different normal and tangential load forms, the calculations of both models match well. The largest induced y-velocities are present inside the rotor, and similar results are captured by both models. The y-velocity profiles deviate more for the tangential loading than for the normal loadings, however, still matching well. The normalised RMS does not exceed 0.5% and is an order of magnitude smaller for the y-velocity than for the x-velocity profiles.

A major difference between the calculations of the AC-squared model and the OF model is that the OF model predicts a gradual decrease of the x-velocity in the wake, and the AC-squared model finds a sudden drop, although the minimum velocity in the wake complies well. The vorticity is assumed to be shed in a straight path behind the rotor causing the deficit in x-velocity to be only behind the rotor (similar to a frozen wake model). This causes the wake not to expand as much as predicted by the OF model. The only streamline deflection is due to the induced y-velocity, and this velocity component is modelled well.

To demonstrate the validity of this assumption, a study is performed for various thrust coefficients. The actuator cylinder is loaded with a uniform normal loading on the outer actuator providing a specific thrust coefficient between 0.1 and 0.9. In Figure 9A, the induced x-velocity at y=0 and three different x-locations are presented for various thrust coefficients.

Both codes predict a very similar behaviour, and no significant dependency is identified between the error and the thrust coefficient. The relative error between both codes with respect to the OF results does not exceed 3% where the biggest differences are around $C_T = 0.5$. Although the induced velocity at various locations behind the rotor is captured rather well, the width of the wake calculated by both codes diverge from each other at large thrust coefficients. This is shown in Figure 9B. The width of the wake is quantified by the deflection of the streamlines. This observation might be expected since for heavily loaded cases, $C_T > 0.5$, the straight vorticity shedding is less applicable. More wake expansion is expected. The relative error is identified to raise from 0.1% for low thrust coefficient up to 12% at high thrust coefficients. Note that the kink around $C_T = 0.5$ is due to the expression of the Mod-Lin correction.

4 | APPLICATION

To demonstrate the use of the AC-squared model, an application will be presented, and the results will be compared with solution of a free wake vortex method. The application presents the results of two rotors inside each other, as a representation of the double-bladed turbine or the strut-blade model in 2D.

The idea behind the AC model and also the AC-squared model is that it consists of two steps: (1) to determine the flow field when the force field is known and (2) determine the force field when the flow field is known. So far in this paper, the force field was prescribed. In this application, an iterative process is implemented between both steps, in which the second step is solved using simple steady blade element theory. The inflow angle and angle of attack at the rotor blades are extracted from the velocity vector at the quarter-chord point of the blades, and this allows to calculate the forces and loading on the rotor. The velocity at every point in the 2D space will be updated, and the process repeated until the model converges to a steady solution. In Figure 10, the sign convention is presented.

4.1 | Effect of inner rotor

To identify the effect of the inner rotor on the outer rotor, a representative example is presented. In this example, an outer rotor with a solidity σ of 0.1 and tip speed ratio λ of 3.0 is selected. The radius of the inner rotor is half of the radius of the outer rotor. The chord and number of blades of the inner rotor is the same as the outer blades, causing the solidity of the inner rotor to be twice the solidity of the outer rotor. Both rotors are rotating with the same rotational speed. The lift and drag polars used for both blades are $C_l = 1.1 \times 2\pi\alpha$ and $C_d = 0$.

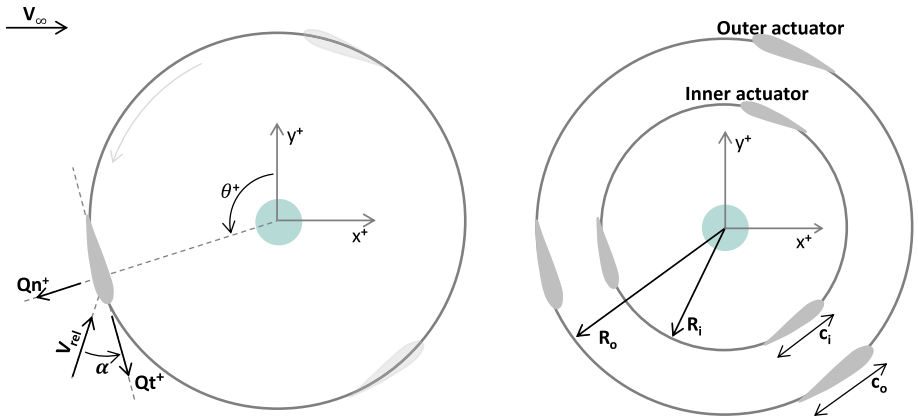

FIGURE 10 Rotor-in-rotor flow model and sign convention [Colour figure can be viewed at wileyonlinelibrary.com]

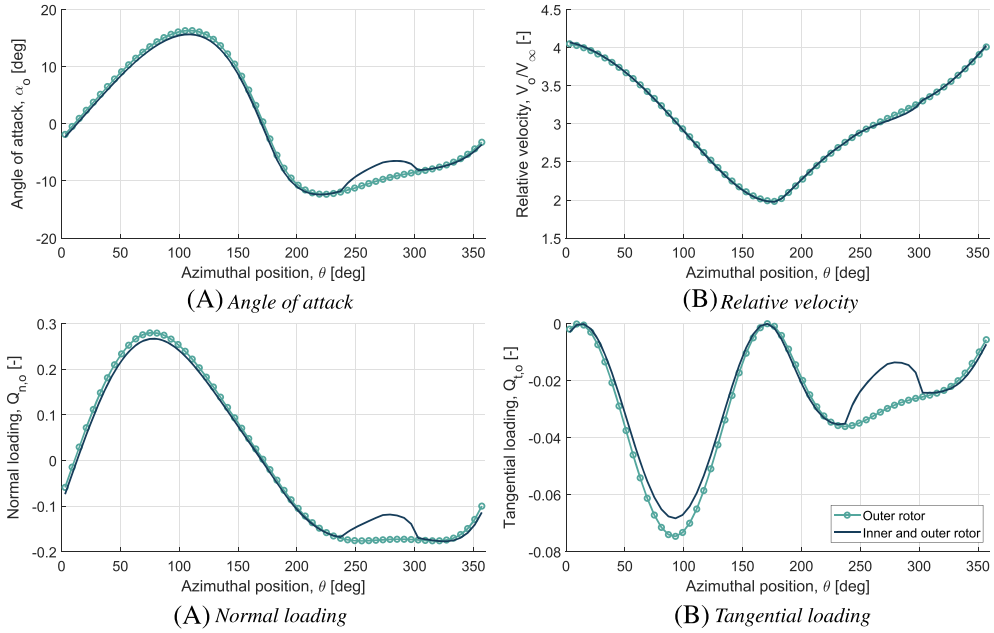

FIGURE 11 Angle of attack, relative velocity, normal, and tangential loading versus the azimuthal position for an actuator-in-actuator concept. Outer rotor: solidity 0.1, tip speed ratio 3, radius 1m. Inner rotor: solidity 0.2, tip speed ratio 1.5, radius 0.5 m [Colour figure can be viewed at wileyonlinelibrary.com]

In Figure 11, the results calculated with the AC-squared model are presented. Figure 11A to Figure 11D display the angle of attack, relative velocity, normal loading and tangential loading as a function of the azimuthal position of the blade. The results are presented both with and without the absence of the inner rotor. From the results, it is clear that the presence of the inner rotor mainly effects the downwind part of the rotor. In the region behind the rotor, the velocity field is affected as such that the angle of attack is decreased and consequently also the loading. The upwind part is only marginally affected.

4.2 | Comparison against U2DiVA calculations

The actuator-in-actuator model is compared with the time-dependent U2DiVA code. In Figure 12 and Figure 13, the angle of attack and relative velocity as a function of the azimuthal position are presented. The first figure presents a low loaded case with a thrust coefficient of 0.54. The second figure represents a highly loaded case with a thrust coefficient of 0.91. Figure 12A and Figure 13A show the operational conditions of the outer rotor, while Figure 12B and Figure 13B present the conditions of the inner rotor. From the comparison, it can be concluded that the AC-squared model is able to predict the overall behaviour both at the outer and inner rotor. Especially for the low loaded case, the differences are minimal. For the more heavily loaded case, the error between both codes is more pronounced, although still acceptable. This is in line with the expectations since it is already noted before that for heavily loaded cases, the wake expands more, which is not captured by the AC model. The discrepancies between both codes are in the same order as in the absence of the inner rotor case (see Ferreira[21]).

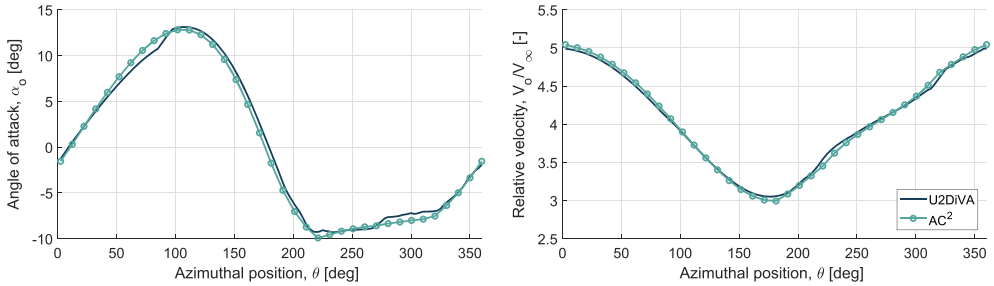

(A) *Angle of attack and relative velocity at outer rotor.*

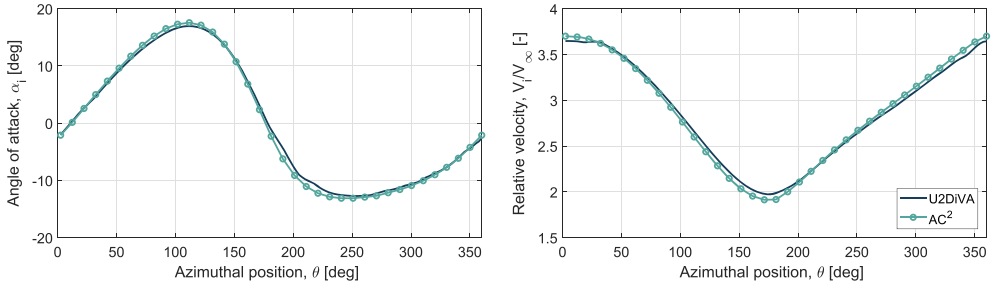

(B) *Angle of attack and relative velocity at inner rotor.*

FIGURE 12 Comparison of angle of attack and relative velocity at inner and outer rotor against U2DiVA. Outer rotor: solidity 0.04, tip speed ratio 4, radius 1m. Inner rotor: solidity 0.03, tip speed ratio 2.8, radius 0.7m [Colour figure can be viewed at wileyonlinelibrary.com]

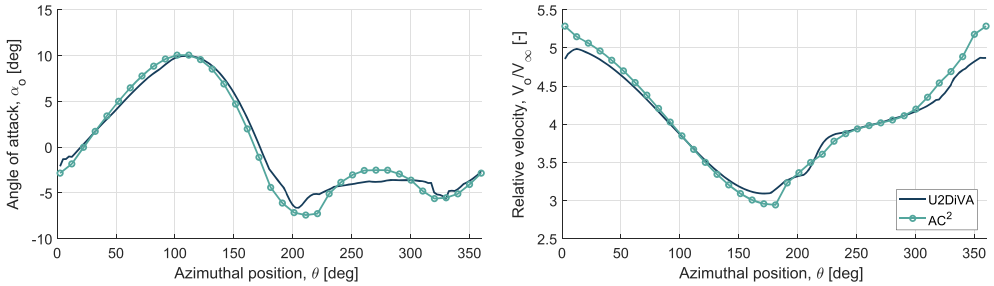

(A) *Angle of attack and relative velocity at outer actuator.*

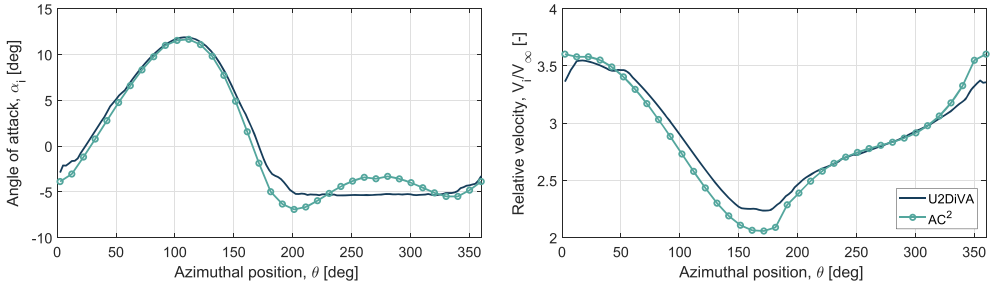

(B) *Angle of attack and relative velocity at inner actuator.*

FIGURE 13 Comparison of angle of attack and relative velocity at inner and outer rotor against U2DiVA. Outer rotor: solidity 0.1, tip speed ratio 4, radius 1m. Inner rotor: solidity 0.07, tip speed ratio 2.8, radius 0.7m [Colour figure can be viewed at wileyonlinelibrary.com]

Furthermore, the operational conditions at the upwind part of both rotors are better predicted than the downwind part. The downwind part is operating inside the wake, which makes it more challenging to compute the induced velocities.

It becomes interesting when considering the power coefficient produced by both rotors separately for various inner rotor radius. Note that a zero inner radius corresponds to the case where the inner rotor is absent. The analysis is presented in Figure 14. The results are presented only for the heaviest loaded case since the differences are more pronounced. First of all, note that the power coefficient at the inner rotor is significantly lower than the outer rotor; however, the inner rotor's power coefficient is increasing with increasing inner radius. The power predicted by the AC-squared model is higher than the one found by the free wake vortex model. This is in agreement with what is found in Ferreira[21] for the original AC model. The difference is smaller for the inner rotor since the loads are significantly lower. A part of the error between both models can be attributed to the lack of modelling the unsteady effects in the AC model.

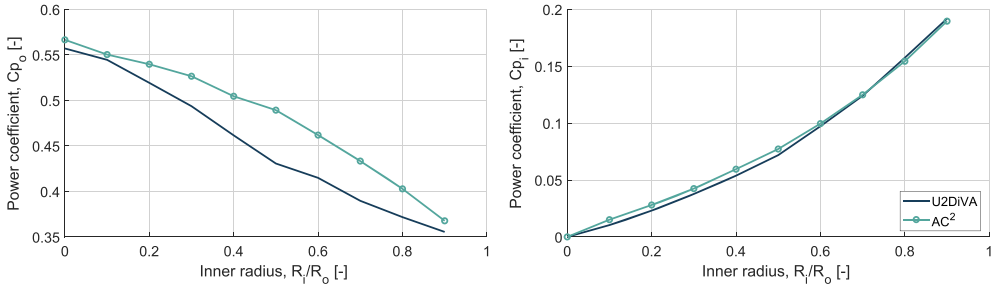

(A) *Outer rotor* (B) *Inner rotor*

FIGURE 14 Comparison of the power coefficient of the inner and outer rotor for various inner radius' against U2DiVA. Outer rotor: solidity 0.1, tip speed ratio 4. Inner rotor: solidity 0.05-0.5, tip speed ratio 0.4-3.6 [Colour figure can be viewed at wileyonlinelibrary.com]

5 | CONCLUSION

In this work, we have worked towards the development of the AC-squared model. This 2D model aims to model the behaviour of two concentric actuator cylinders as a modelling technique for applications such as strut-blade modelling, double-bladed turbines, the so-called butterfly turbine, or even the modelling of the tower.

The AC-squared model is an extension of the original AC model of Madsen.[13] The induced velocity at the 2D field is calculated as a result of the force field acting on the inner and the outer actuator cylinders. The effect of both the normal and tangential loading on the velocity field are incorporated. The *Mod-Lin* correction[13] is applied to account for the non-linear part of the solution.

The implementation of the AC-squared model is first verified using flow cases with analytical solutions and secondly verified against OpenFOAM calculations. The first verification cases consists of the force field acting on a cylinder in freestream, a simplified model of an airfoil in freestream, a conservative force field with only a normal loading on a cylindrical surface and a non-conservative force field with a tangential loading on a cylindrical surface. All cases confirmed a good implementation. The verification of the AC-squared model with laminar OF calculations concluded that the x- and y-velocity match well for all load forms. The induced velocities are captured well by the new model; however, the assumption that the vorticity is shed in a straight path behind the rotor is less valid for highly loaded actuators (ie, high thrust coefficient). In these cases, the wake expands significantly more than for lower loaded cases causing this assumption to be less true.

Finally, an application is provided to demonstrate the use of the actuator-in-actuator cylinder model. In this application, the prescribed loading is replaced by an iterative process that calculates the loading at the rotor based on the relative velocity and angle of attack. The effect of the inner rotor on the outer rotor is clearly identifiable, and the results are compared with the vortex/panel method U2DiVA.

ACKNOWLEDGEMENTS

The authors would like to thank Andrés Meana Fernández for his input to set up the OpenFOAM model. We would also like to express our appreciation to Bruce LeBlanc for the useful discussions on the topic and review of the article.

ORCID

Delphine De Tavernier https://orcid.org/0000-0002-8678-8198

REFERENCES

1. Paulsen US, Borg M, Madsen HA, et al. Outcomes of the deepwind conceptual design. *Energy Procedia*. 2015;80:329-341.
2. Ferreira CS, Madsen HA, Barone M, Roscher B, Deglaire P, Arduin I. Comparison of aerodynamic models for vertical axis wind turbines. *J Phys Conf Ser*. 2014;524:012125.
3. Ferreira CS, Scheurich F. Demonstrating that power and instantaneous loads are decoupled in a vertical-axis wind turbine. *Wind Energy*. 2014;17(3):385-396.
4. Rezaeiha A, Kalkman I, Blocken B. CFD simulation of a vertical axis wind turbine operating at a moderate tip speed ratio: guidelines for minimum domain size and azimuthal increment. *Renew Energy*. 2017;107:373-385.
5. Siddiqui MS, Durrani N, Akhtar I. Numerical study to quantify the effects of struts and central hub on the performance of a three dimensional vertical axis wind turbine using sliding mesh. Volume 2: Reliability, Availability and Maintainability (RAM); Plant Systems, Structures, Components and Materials Issues; Simple and Combined Cycles; Advanced Energy Systems and Renewables (Wind, Solar and Geothermal); Energy Water Nexus; Thermal Hydraulics and CFD; Nuclear Plant Design, Licensing and Construction; Performance Testing and Performance Test Codes; 2013.
6. Mendoza V. Aerodynamic studies of vertical axis wind turbnes using actuator line model. *PhD Thesis*: Acta Universitatis Upsaliensis; 2018.
7. Moran WA. Giromill wind tunnel test and analysis. *Report*, U.S. Energy Research and Development Administration; 1977.
8. Goude A. Fluid mechanics of vertical axis turbines - simulations and model development. *PhD thesis*: Acta Universitatis Upsaliensis; 2012.

9. Hara Y, Kawamura T, Akimoto H, Tanaka K, Nakamura T, Mizumukai K. Predicting double-blade vertical axis wind turbine performance by a quadruple-multiple streamtube model. *Int J Fluid Mach Syst*. 2014;7(1):16-27.
10. Madsen HA. The Actuator Cylinder - a flow model for vertical axis wind turbines. The institute of industrial constructions and energy technology; 1982.
11. Ning A. Actuator Cylinder theory for multiple vertical axis wind turbines. *Wind Energy Sci*. 2016;1(2):327-340.
12. Li A. Double actuator cylinder (AC) model of a tandem verticalaxis wind turbine (VAWT) counter-rotating rotor concept operating in different wind conditions. *Msc thesis*: Technical University of Denmark; 2017.
13. Madsen HA. On the ideal and real energy conversion in a straight bladed vertical axis wind turbine. *PhD thesis*: Institute of Industrial Constructions and Energy Technology, Aalborg University Centre; 1983.
14. Froude RE. On the part played in propulsion by differences of fluid pressure. *Trans Inst Nav Archit*. 1889;30:390.
15. Katz J, Plotkin A. *Low Speed Aerodynamics*. 2nd ed. United States of America: Cambridge University Press; 2001.
16. Madsen H, Larsen T, Vita L, Paulsen U. Implementation of the Actuator Cylinder flow model in the HAWC2 code for aeroelastic simulations on vertical axis wind turbines. In: 51st AIAA Aerospace Sciences Meeting including the New Horizons Forum and Aerospace Exposition (2013-0913); 2013; Grapevine, TX, United States.
17. Madsen HA, Paulsen US, Vita L. Analysis of VAWT aerodynamics and design using the actuator cylinder flow model. *J Phys Conf Ser*. 2014;555:012065.
18. Cheng Z, Madsen HA, Gao Z, Moan T. Aerodynamic modeling of floating vertical axis wind turbines using the Actuator Cylinder flow method. *Energy Procedia*. 2016;94:531-543.
19. The OpenFOAM Foundation Ltd. OpenFOAM v6. https://openfoam.org; 2018.
20. Ferreira CS. The near wake of the VAWT. *PhD thesis*: Delft University of Technology; 2009.
21. Ferreira CS, Geurts B. Aerofoil optimization for vertical-axis wind turbines. *Wind Energy*. 2015;18(8):1371-1385.

How to cite this article: De Tavernier D, Ferreira C. An extended actuator cylinder model: Actuator-in-actuator cylinder (AC-squared) model. *Wind Energy*. 2019;1–13. https://doi.org/10.1002/we.2340